First measurements of near threshold J/ψ photoproduction

(GlueX Collaboration)

(Dated: March 14, 2019)

We report on the measurements of the $\gamma p \to J/\psi p$ cross-section from 11.8 GeV down to the threshold of 8.2 GeV beam energy from the GlueX experiment using tagged photon beam. We measure a t-slope of this reaction of $1.665 \pm 0.347 \pm 0.079$ at 10.7 GeV average energy. The total cross-section when compared to theoretical predictions shows domination of three-gluon exchange below 10.7 GeV. The LHCb pentaquark candidates can be produced in the s-channel in this reaction, and we see no evidence for them. We set a model dependent upper limit on $\mathcal{B}(P_c^+(4450) \to J/\psi p)$ of 1.01% (at 90% C.L.).

INTRODUCTION

The upgraded 12 GeV Jefferson Lab accelerator has the unique opportunity - correct energy, high intensity, and polarized beams - to study the J/ψ photoproduction right above the threshold (at a beam energy of $E_\gamma = 8.2$ GeV) up to the maximum accelerator energy. The main interest in these studies comes from their direct relation to the two pentaquarks, $P_c^+(4380)$ and $P_c^+(4450)$, reported by LHCb [1] in the $J/\psi p$ channel of the $\Lambda_b^0 \to J/\psi K^- p$ decay. The existence of these resonances implies they should be seen also in the s-channel photoproduction:

$$\gamma p \to P_c^+ \to J/\psi p \tag{1}$$

at 10 GeV beam energy. Almost immediately after the pentaquarks have been reported it was realized [2–4] that the $P_c^+ \to J/\psi p$ decay plus its time inversion and the addition of the $J/\psi - \gamma$ coupling based on the Vector Meson Dominance (VMD), gives the above reaction (1). The Breit-Wigner expression for the cross-section includes the measured width of the pentaquark, the VMD coupling obtained from the leptonic decay of the J/ψ, and the only unknown parameter, the branching fraction of the $P_c^+ \to J/\psi p$ decay, that enters squared. Thus, by measuring the J/ψ photoproduction cross-section one can estimate this branching fraction.

The near threshold charmonium exclusive production is an excellent probe to study the color charge distribution of the proton, which is another important aspect of the presented measurements. A heavy quark system like J/ψ interacts with the light quark proton via gluon exchange. Based on the dimensional scaling rule the near threshold cross-section behavior (up to a normalization coefficient) was predicted [5] depending on the number of gluons exchanged in the reaction. At high energies one-gluon exchange is preferable (plus soft gluons needed to make colorless final state), while near threshold all the partons should participate requiring more high-x gluons to be involved. In [6] it is argued that the t-dependence of the exclusive reaction is defined by the proton gluonic form-factor for which, in analogy with the electromagnetic form factors, we can assume a dipole form:

$$F(t) \ \sim \ 1/(1 - t/m_0^2)^2, \tag{2}$$

though with a different mass scale m_0. According to [7] the J/ψ photoproduction near threshold is dominated by the real part of the $J/\psi p$ elastic amplitude, which is critically important since it contains a term (trace anomaly) related to the fraction of the nucleon mass arising from gluons. In [8] it was demostrated that the shape of the cross-section energy and t-dependence is most sensitive the gluon contribution to the nucleon mass in the near threshold region.

We report on the first measurements of the J/ψ photoproduction cross-section from the threshold up to 11.8 GeV beam energy. This energy range was poorly covered by previous old experiments, while our measurements are the first that extend close to the threshold. The only published result in this region is at 11 GeV from the Cornell experiment [9]. It has been done on a Be target registering only the electron-positron pair from the J/ψ decay in electro-magnetic calorimeters. Measurements at SLAC [10] have been done on a deuterium target at photon energies of 13 GeV and above, but only in the forward ($t = t_{min}$) region due to the narrow acceptances of the two spectrometers used in the experiment. In addition, at 19 GeV, the t-dependence of the cross-section has been scanned.

We have measured the exclusive reaction $\gamma p \to J/\psi p$, where J/ψ is identified by its decay into electron-positron pair. The cross-section is normalized using the Bethe-Heitler process $\gamma p \to e^+ e^- p$. The data were collected during the GlueX experiment running in Hall D of Jefferson Lab in years 2016 and 2017, which represents about 25% of the total statistics accumulated so far.

THE EXPERIMENT

The GlueX experiment uses linearly-polarized tagged-photon beam produced by the 12 GeV Continuous Electron Beam Accelerator Facility (CEBAF). The electron beam incident on a thin diamond radiator produces Bremssstrahlung spectrum with a coherent peak adjusted in the energy range of $8.2-9$ GeV, where the photons are also polarized. For the present analysis the polarization is not of interest and we are using also data from amorphous radiator. The scattered electron after passing a

9 Tm dipole magnet, is registered in a tagging scintillator array allowing to determine the photon energy with a resolution better than 0.3%.

The photon beam is collimated (5 mm diameter hole) at a distance of 75 m from the radiator, where it enters the experimental hall. There the photon flux and energy is monitored by a electron-positron pair spectrometer system.

The GlueX detector is based on a $2T$ 4m-long solenoid magnet and has full azimuthal and $1 < \theta < 120°$ polar angle coverage. A 30 cm long liquid Hydrogen target is placed inside the solenoid. Tracking around the target is performed by the Central Drift Chamber (CDC) system: $3,500$ straw tubes, each 1.5 m long, grouped in layers with axial and stereo orientation. In forward direction, where the track density is higher, planar drift chambers with both wire and cathode strip readout are used. The Forward Drift Chamber (FDC) system consist of 24 such disk-shape chambers grouped in four packages on a total distance of 2 m at the downstream end inside the magnet, totaling of about $12,500$ readout channels. The two drift chamber systems are surrounded by a lead-scintillator electromagnetic barrel calorimeter (BCAL). Electronically the calorimeter is grouped in 192 azimuthal segments and four radial layers allowing to reconstruct both transverse and longitudinal shower development.

The detector hermeticity in forward direction outside of the magnet is achieved by the Time of Flight (TOF) scintillator wall and the Forward Calorimeter (FCAL), both placed at ~ 6 m from the target. The FCAL is a lead-glass electromagnetic calorimeter consisting of $2,800$ blocks. Both calorimeters, FCAL and BCAL, are used to trigger the detector readout requiring enough energy deposition in one of them separately or in total.

The intensity of the beam above the J/ψ threshold was $\sim 2\ 10^7$ photons/s in 2016 and first period of 2017, then increased up to $\sim 5\ 10^7$ photons/s for the rest of 2017, resulting in a total accumulated luminosity of 68 pb^{-1}. In 2016 the maximum tagged photon energy was 11.85 GeV, while for the later running it was lowered to 11.4 GeV.

We study the exclusive reaction $\gamma p \to pe^+e^-$ in the region of the e^+e^- invariant mass, $M(e^+e^-)$, above 0.9 GeV, that includes ϕ, J/ψ peaks, as well as Bethe-Heitler (BH) process as a continuum. For illustration Fig.1 shows the $M(e^+e^-)$ spectrum from our data applying all the cuts and analysis procedures as explained below. We use BH in the invariant mass region of $1.2 - 2.5$ GeV for the absolute normalization of the J/ψ total cross-section, thus eliminating uncertainties from factors like luminosity and common detector efficiencies.

From experimental point of view, the most challenging is the suppression of the pion background that is about $3 - 4$ orders of magnitude higher than the electron/positron signal in the BH continuum. This is achieved mainly by applying p/E cuts for both electron and positron candidates, where the particle momentum p

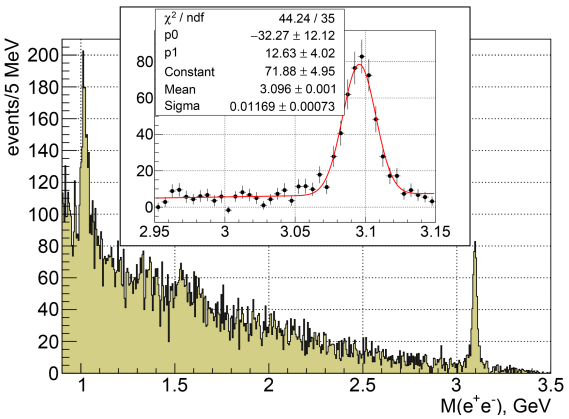

FIG. 1: Electron-positron invariant mass spectrum obtained from the data. Zoomed J/ψ invariant mass region, shown as an insert, is fitted with linear background plus a Gaussian.

comes from the kinematic fit as explained below and E is the energy deposition in the calorimeters. We apply 2σ cut, $p/E < \langle p/E \rangle + 2\sigma$, on both leptons, where the mean $\langle p/E \rangle$ is close to unity and the calorimeter resolution σ for the sample of electrons/positrons in the BH region is 3.9% for FCAL and 6.8% for BCAL. In addition, we take advantage of the layer structure of BCAL using the energy deposited in the inner-most layer, E_{pre}, and require for electrons/positrons to have $E_{pre} sin\theta > 30 MeV$ (sin of polar angle θ takes into account the pathlenght along the calorimeter), thus cutting significant fraction of pions that normally have low energy deposition. We exclude also small momenta (< 0.4 GeV) for the two leptons where pions are dominating, and for the proton where it is poorly reconstructed. Due to the steeper t-dependence of the BH process compared to the pion production, to minimize the pion background when using BH for normalization, we select only the low t region, $-(t - t_{min}) < 0.6$ GeV^2.

The protons up to ~ 1 GeV are identified by their higher energy deposition in the drift chambers, while for higher momenta all the particle type hypotheses are included as possible combinations. The timings of the three final state particles are required to be within the same electron beam bunch (± 2 ns for most of the data). The tagged beam photons that are in time with this bunch are selected as possible candidates associated with the reaction, which contain photons accidentally associated. The accidental photons are subtracted statistically by selecting a sample of photons that are out-of-time with respect to reaction beam bunch.

Taking advantage of the exclusivity of the reaction and the precise knowledge of the beam energy we use a kinematic fit to improve the resolution of the measured particle momenta and angles. The fit takes into account momentum and energy conservation, as well as requires com-

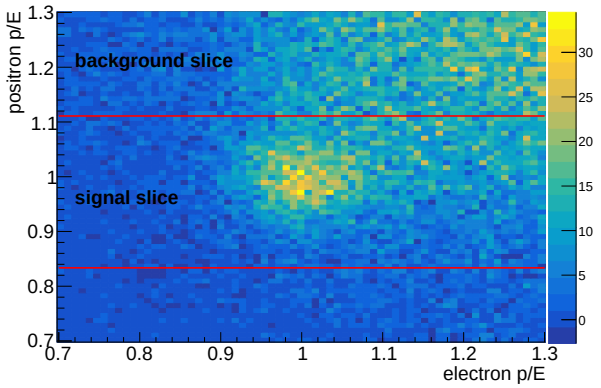

FIG. 2: Electron vs positron p/E distribution in the invariant mass region of $1.2 - 2.5$. Note, we use the inverse of E/p usually used for e/π separation. Drawn are the cuts that separate the signal and background slices as they are used to extract the BH yield.

mon vertex for the three final state particles. Loose cuts are applied on the χ^2 of the fit, as well as on the missing mass squared and the missing transverse momentum of the reaction. The electron-positron invariant mass spectrum in Fig.1 is obtained using the fitted quantities. This allows us to achieve ~ 12 MeV mass resolution for J/ψ. Studies of the kinematic fit show that it is constrained mainly by the proton angle and momentum and the angles of the two leptons. Due to the poorer reconstruction of the lepton momenta in the solenoid field especially in forward direction they do not affect noticeably the kinematic fit.

We extract the J/ψ and the BH yields in bins of beam energy or t. Fig.2 shows the electron vs positron p/E distribution in the BH continuum region. One can clearly see the lepton peak sitting on pion background. The BH yield is extracted from slices of the $2D$-distribution projected on one of the leptons: one slice that includes the signal and another one for the background outside of the peak. The background slice is normalized by fitting it to the signal slice (with an addition of a Gaussian) and then subtracted from the signal slice. We estimate 54% pion contamination for 2σ cut on the signal in the BH continuum region of $1.2 < M(e^+e^-) < 2.5$. The J/ψ yield is obtained by fitting the invariant mass spectrum (as in Fig.1) with a Gaussian and linear background. For that we use binned likelihood method within the RooFit package.

We have performed Monte Carlo (MC) simulations of the J/ψ production, as well as the BH continuum. The generated events were passed through the GlueX detector model using Geant3 package and then analyzed in the same way as the data. Accidental tagger hits as well as out-of-time detector hits extracted from the data, are injected into the generated events. The BH electromagnetic diagrams can be calculated exactly in principle. We have used two BH generators, one based on analytical calculations [11] and another one [12] on numerical calculations of the diagrams, giving very similar results. We generate the J/ψ-proton final state using an exponential t-dependence and a cross-section as a function of the beam energy as obtained from this experiment. Then J/ψ decays assuming helicity conservation. We use MC to calculate the BH and J/ψ efficiencies, ε_{BH} and $\varepsilon_{J/\psi}$.

RESULTS AND DISCUSSIONS

We calculate the total cross-section as a function of beam energy using the following formula:

$$\sigma(E) = \frac{N_{J/\psi}(E)}{N_{BH}(E)} \frac{\sigma_{BH}(E)}{\mathcal{B}_{J/\psi}} \frac{\varepsilon_{BH}(E)}{\varepsilon_{J/\psi}(E)} \quad (3)$$

Here $N_{J/\psi}$ and N_{BH} are the J/ψ and BH yields, σ_{BH} – BH cross-section calculated using MC, and $\mathcal{B}_{J/\psi}$ – $J/\psi \to e^+e^-$ branching ratio of 5.97%. Note that the result depends only on the relative BH to J/ψ efficiency and the flux that varies significantly with the beam energy cancels out in the yield ratio.

In this paper we show results for the differential cross-section in bins of t averaged in the energy region of $10 < E_\gamma < 11.8$ GeV. Closer to the threshold, due to the strong variation of t_{min} and the t-range, such analysis require slices in beam energy for which we don't have enough statistics. Away from the threshold the beam flux is not correlated with t and for the differential cross-section we don't use BH for normalization. Another reason is that the high-t BH region is dominated by pions which results in additional uncertainties for the extracted t-slope.

The total cross-section in bins of beam energy and the differential cross-section as function of $-(t - t_{min})$ are shown in Tables I and II together with the statistical and point-to-point systematic errors. Table III summarizes our estimate of the systematic errors for the overall cross-section normalization. The main contribution comes from possible uncertainty in the relative BH to J/ψ efficiency. This estimation is based on comparison between the calculated and extracted from the data BH cross-section as function of different kinematic variables that bridge the BH and J/ψ kinematic regions. Note however, that such comparison can be done as a function of a single variable only. For example, to have an overlap of both proton angle and momentum requires BH invariant mass to approach the J/ψ mass where the BH cross-section is very small and contaminated with pions.

The external radiation of the electrons is part of the Geant simulation. The internal radiation was included in the simulations of the J/ψ decay using the PHOTOS code [13]. The results show that the kinematic fit recovers the electron-positron invariant mass before the radiation, as expected due to the dominant constraint to the

Energy bin, GeV	σ,nb	stat error	p.t.p. syst.
8.2-8.56	0.11592	0.03140	0.01158
8.56-8.92	0.34317	0.06667	0.03448
8.92-9.28	0.31308	0.12709	0.03839
9.28-9.64	0.83483	0.19420	0.08143
9.64-10	0.86836	0.19636	0.10628
10-10.36	0.94905	0.18733	0.05122
10.36-10.72	1.38315	0.28426	0.13604
10.72-11.08	1.27357	0.20634	0.13722
11.08-11.44	2.15758	0.42126	0.31749
11.44-11.8	3.24452	0.92849	0.32437

TABLE I: Total cross-section, statistical and point-to-point systematic errors in bins of beam energy.

fit from the proton that is decoupled from the J/ψ decay. This is not the case for the BH process where the electron-positron pair and the recoil proton are part of the same reaction. In [14] the radiative corrections to the BH process are calculated as a function of the cut on the photon energy, however there is an ambiguity how this energy is distributed between the final state particles. In the extreme case we assume that the electron-positron invariant mass is not affected and the radiative effects are compensated by the proton, resulting in an upper limit of 8.3% for the BH radiative correction. The maximum effect of the ρ' production was estimated by comparing the results for two invariant mass ranges: $1.2-2$ and $2-2.5$ GeV. Based on [11] the contribution of the Timelike Compton Scattering is estimated to be less than 4%. Due to uncertainties of the GPD model we doubled this systematic error.

As a cross-check we have compared the cross-sections obtained from the 2016 and 2017 data sets separately, representing different experimental conditions (solenoid field, intensity, beam spectrum). They are statistically consistent in bins of energy with an average ratio of 0.96 ± 0.25. Based on the missing mass we can set an upper limit for the target excitation contribution, $\gamma p \to J/\psi p\pi$, of 5%. The point-to-point systematics was evaluated by varying the procedures for fitting the J/ψ peak in the invariant mass spectrum and the BH electron/positron peak in the p/E distribution. We have varied also the BH invariant mass range used for normalization. The uncertainties of the parameters used in the J/ψ simulations (t-slope, energy dependence) have smaller effect on the p.t.p. uncertainties.

In Fig.3 we show the t-dependence of the differential cross-section for beam energies of $10-11.8$ GeV with an average of 10.72 GeV. We obtain a t-slope of $1.665 \pm 0.347 \pm 0.079$ GeV^{-2}, to be compared with the Cornell result [9] at $E_\gamma = 11$ GeV of 1.25 ± 0.2 GeV^{-2} and the SLAC result [10] at $E_\gamma = 19$ GeV of 2.9 ± 0.3 GeV^{-2}. All these results are consistent with the hypothesis [6] for a dipole t-dependence (Eq.(2)) of the differential cross-section with a mass scale of 1.14 GeV.

$-(t-t_{min})$ bin, GeV^2	$d\sigma/dt$,nb/GeV^2	stat error	p.t.p. syst.
0-0.15	1.64311	0.33380	0.02922
0.15-0.3	1.24903	0.26483	0.01501
0.3-0.45	1.08834	0.24788	0.01196
0.45-0.6	0.62749	0.18202	0.01255
0.6-0.75	0.59858	0.16282	0.02148
0.75-0.9	0.46977	0.14484	0.00495
0.9-1.05	0.39982	0.13441	0.00604

TABLE II: Differential cross-sections, statistical and point-to-point systematic errors in bins of $-(t-t_{min})$.

Origin	Estimate, %
$\varepsilon_{BH}/\varepsilon_{J/\psi}$ relative efficiency	23
Radiative corrections	8.3
TCS contribution to BH	8
ρ' contribution to BH	7
total	26.7

TABLE III: Systematic errors

The GlueX total cross-section in bins of beam energy is shown in Fig.4. In the same figure the Cornell [9] and SLAC [10] measurements are plotted. Note that the SLAC experiment measured $d\sigma/dt$ at $t = t_{min}$. In order to estimate the total cross-section, we have integrated over t assuming dipole t-dependence, Eq.(2) $m_0 = 1.14$ GeV. We have fitted the theoretical predictions of [5] with two parameters being the amplitudes of the two-gluon and three-gluon exchange cross-sections, to the GlueX data only. We have used again Eq.(2) for the gluonic from-factor $F(t)$ that enters in Eqs.(3) and (4) in [5], in contrast to the paper where $F(t)^2 = exp(1.13t)$ is assumed. One can see that the three-gluon exchange starts dominating below ~ 10.5 GeV when approaching the threshold. This is consistent with the fact that at

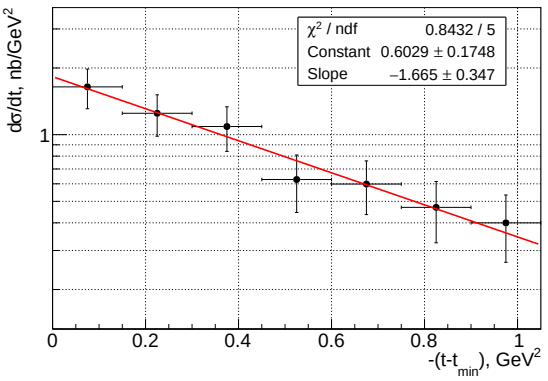

FIG. 3: Differential cross-section from this work as function of $-(t-t_{min})$ for $\langle E_\gamma \rangle = 11.72$ GeV.

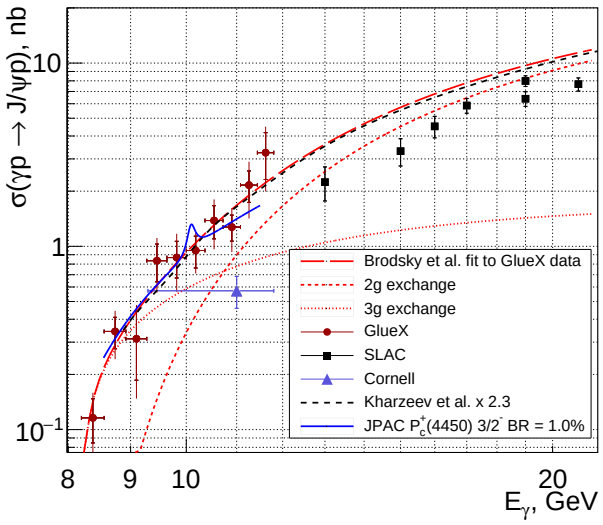

FIG. 4: GlueX results for the J/ψ total cross-section vs beam energy, compared to the Cornell [9] and SLAC [10] results and also to the theoretical predictions [5, 7], and JPAC model [4] correspoding to the upper limit of $\mathcal{B}(P_c^+(4450) \to J/\psi p) = 1.01\%$ for spin-3/2 case as discussed in the text.

threshold all the constituents should participate in the reaction. We have plotted also the theoretical curve from [7] multiplied by a factor of 2.3 to fit our data (according to the authors there is up to a factor of three uncertainty in the normalization). The model [7] predicts a high gluonic contribution to the nucleon mass, however, despite of the agreement with the data, the sensitivity to this contribution has to be studied with higher statistics including the near threshold t-dependence. The GlueX cross-section is about three times higher than the Cornell [9] and a factor of ~ 1.5 above the SLAC [10] result if compared to the Brodsky et al. curve fitted to the GlueX data. It exibits a less steep behavior near threshold compared to what was suggested by the old measurements.

Since the LHCb pentaquark P_c^+ states are produced in the s-channel, they should show up as peaks at $E_\gamma \sim 10$ GeV in the cross section in Fig.4. We see no evidence for such peaks, although the $P_c^+(4380)$ has a large width of ~ 1 GeV in E_γ, and we have little sensitive to its production with the current precision of our data. We set upper limits on $\mathcal{B}(P_c^+(4450) \to J/\psi p)$ by fitting our data with a variation of the model described in [4] where the non-resonant component is described by a combination of Pomeron and tensor amplitudes, in analogy to the two-gluon and three-gluon amplitudes described above. The upper limits at 90% confidence level determined by integrating the likelihood curve of the model fit, are 1.01% and 0.18%, assuming the $P_c^+(4450)$ is spin-3/2 or spin-5/2, respectively. The spin-3/2 case is plotted on Fig.4. A less model-dependent limit is found using the incoherent sum of a Breit-Wigner and the non-resonant component as desribed above. Applying the same likelihood procedure yields an upper limit at 90% confidence level of $\sigma(\gamma p \to P_c^+(4450)) \times \mathcal{B}(P_c^+(4450) \to J/\psi p) < 0.65$ nb.

[1] R. Aaij et al. (LHCb collaboration), Phys. Rev. Lett. **115**, 072001 (2015).
[2] V. Kubarovsky and M. B. Voloshin, Phys. Rev. D **92**, 031502 (2015).
[3] M. Karliner and J. Rosner, Phys. Lett. B **752**, 329 (2016).
[4] A. Blin, C. Fernandez - Ramirez, A. Jackura, V. Mathieu, V. Mokeev, A. Pilloni, and A. Szczepaniak, Phys. Rev. D **94**, 034002 (2016).
[5] S. Brodsky, E. Chudakov, P. Hoyer, and J. Laget, Phys. Lett. B **498**, 23 (2001).
[6] L. Frankfurt and M. Strikman, Phys. Rev. D **66**, 031502 (2002).
[7] D. Kharzeev, H. Satz, A. Syamtomov, and G. Zinovev, Nucl.Phys. A **661**, 568 (1999).
[8] Y. Hatta and D.-L. Yang, //arxiv.org/pdf/1808.02163.pdf (2018).
[9] B. Gittelman, K. M. Hanson, D. Larson, E. Loh, A. Silverman, and G. Theodosiou, Phys. Rev. Lett. **35**, 1616 (1975).
[10] U. Camerini, J. Learned, R. Prepost, C. Spencer, D. Wiser, W. Ash, R. L. Anderson, D. M. Ritson, D. Sherden, and C. K. Sinclair, Phys. Rev. Lett. **35**, 483 (1975).
[11] E. Berger, M. Diehl, and B. Pire, Eur.Phys.J.C **23**, 675 (2002).
[12] R. Jones, private communication (2018).
[13] E. Barberio et al. , Comput.Phys.Commun. **79**, 291 (1994).
[14] M. Heller, O. Tomalak, and M. Vanderhaeghen, Phys. Rev. D **97**, 076012 (2018).

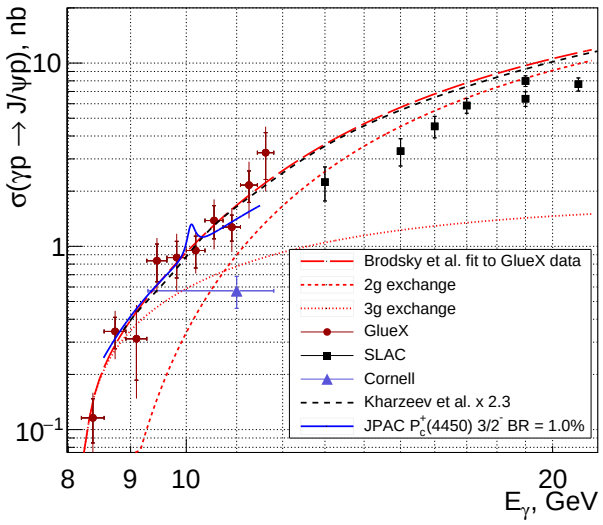
σ(γp → J/ψp), nb
10
1
10⁻¹
8
9
10
20
Eγ, GeV
Brodsky et al. fit to GlueX data
2g exchange
3g exchange
GlueX
SLAC
Cornell
Kharzeev et al. x 2.3
JPAC P_c^+(4450) 3/2^- BR = 1.0%

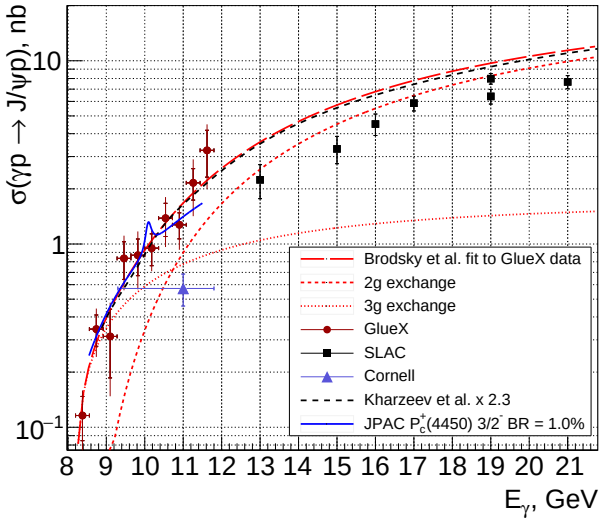
σ(γp → J/ψp), nb
10
1
10⁻¹
8 9 10 11 12 13 14 15 16 17 18 19 20 21
Eγ, GeV
Brodsky et al. fit to GlueX data
2g exchange
3g exchange
GlueX
SLAC
Cornell
Kharzeev et al. x 2.3
JPAC P_c^+(4450) 3/2^- BR = 1.0%